Technical Theme Topics

Christos Christopoulos, Associate Editor

Coupling and Emissions Under Cyclostationary Conditions

For convenience, engineers often make the assumption that the statistical behaviour of signals remains constant in time (time-invariant). However, as the complexity of modern systems increases and the simultaneous presence of several clocked sources of EMI, this assumption is not always valid. Cyclostationary signals have hidden periodicities in the way they transport electromagnetic energy. Cyclostationarity was first studied in connection with mechanical signals. Studying them in connection with EMC is used in identifying patterns of emission from specific areas of PCBs and therefore can assist in taking appropriate remedial actions.

The paper by *Kuznetsov et al* presents an analysis of electrical signals through a process of statistical cyclic averaging to characterize the emission properties for EMC analysis and design. Experimental results are also presented in support of the theoretical analysis.

In future issues of the EMC Magazine we will cover topics such as the Electrical Behavior of CFCs, Stochastic EMC Applications, and Lightning Characterization.

Cyclostationary Characterization of Radiated Emissions in Digital Electronic Devices

Yury V. Kuznetsov, Senior Member, IEEE; Andrey B. Baev, Senior Member, IEEE; Maxim A. Konovalyuk (konovaluk@mai-trt.ru); Anastasia A. Gorbunova (gorbunova@mai-trt.ru); Johannes A. Russer, Member, IEEE; Peter Russer, Life Fellow, IEEE

Abstract— Stochastic electromagnetic fields originating from processes in digital circuitry affect the operation of the circuit, increase the error rate in the transmission of digital signals, degrade the circuit's performance, yield malfunction of the system or even lead to a complete failure of the system's operation. Interference from stochastic fields are not only disruptive but are becoming more common due to the increasing complexity of modern electronics. Stochastic electromagnetic fields under common circumstances are due to a mixture of emissions from different sources, which makes a quantification of stochastic fields very challenging. Since digital signals are clocked, the ensemble averages of the electromagnetic field transients representing the digital signal exhibit a periodic time dependence with the period of the clock interval. The probabilistic model of the cyclostationary random process was composed by appropriate transformations of the initial discrete random process of the binary symbols. Exploiting the cyclostationary characteristics of stochastic fields greatly simplifies their analysis. The physical signal propagating along the transmission line is considered also a source of the radiating electromagnetic field which preserves the cyclostationary properties of the binary sequence. The stochastic process of the measured near-field emissions inherits probability characteristics from the random process of the physical signal in the transmission line. This paper presents an approach for quantifying emissions and coupling of stochastic fields using their cyclostationary properties.

For practical evaluation of cyclostationary characteristics the statistical cyclic averaging of the measured signals are used. The important feature of the statistical cyclic averaging procedure is its capability to distinguish cyclostationary signals from a mixture of stochastic processes such as stationary noise with deterministic signals and even from other cyclostationary signals with distinct cyclic frequencies. The measurement setup for observing electromagnetic emissions from printed circuit boards (PCBs) hosting digital electronic devices comprises an automated positioning system with a scanning near-field probe attached to the moving scanner head. This scanning near-field probe and a properly position fixed or also movable reference probe are connected to the inputs of a multi-channel digital oscilloscope for simultaneous and synchronous sampling and registering of the magnetic field components. The registered data from the oscilloscope was transferred to a data acquisition computer. After the postprocessing procedure, the spatial localization of distributed radiating sources on the surface of the PCB was performed in conjunction with determination of their average power characteristics and specified cyclic frequencies. The proposed cyclic averaging was applied to the spatial separation of radiating sources with different bit rates and for the quantitative characterization of crosstalk and coupling between transmission lines carrying the data sequences

Y.V. Kuznetsov, A.B. Baev, M.A. Konovalyuk, and A.A. Gorbunova are with the Theoretical Radio Engineering Department, Moscow Aviation Institute (National Research University), Volokolamskoe shosse, 4, Moscow, 125993, Russian Federation (e-mail: kuznetsov@ieee.org; baev@mai.ru).
J.A. Russer, and P. Russer are with the Technische Universität München, Arcisstrasse, 21, 80333, Munich, Germany, (e-mail: jrusser@tum.de).

and subsequent estimation of bit error rate (BER) caused by the crosstalk using their cyclostationary properties.

Index Terms—Cyclostationarity, electromagnetic interference, near-field scanning, stochastic electromagnetic fields, spatial-time source localization

I. Introduction

The trend in modern electronic systems is towards high bandwidths, high data rates, small dimensions and low power levels. Radiated and conducted electromagnetic interference (EMI) impinging from external sources but also originating from signal transients inside the circuit may affect the circuit, resulting in an increased error rate, degraded performance, or yielding malfunction of the system and even completely failure of the system operation. Due to the increasing complexity and package density of modern digital electronic circuitry this problem is growing in importance. To ensure signal integrity in electronic systems an EMI-aware circuit and system design is required [1]-[6]. Interference from stochastic fields are not only disruptive but are becoming more common due to the increasing complexity of modern electronics. Stochastic fields under common circumstances are due to a mixture of emissions from different sources, which makes a quantification of stochastic fields very challenging. Stochastic electromagnetic (EM) fields occurring in digital circuitry can be modelled by a random process with cyclostationary properties [7], [8]. Such properties arise due to the regular data generation processes and the deterministic shape of the data pulses defined by the interface procedure inherent to the given communication link of the electronic device (ED) [9]. The signals of high-speed digital electronic circuits can be considered as cyclostationary stochastic signals, since when considered as interfering signals the information carried by the signals is irrelevant. Since the digital signals are clocked, their ensemble averages exhibit a periodic time dependence with the period of the clock interval.

Methods for measuring and modeling EMI radiated from PCBs were described in [10], [11]. It has been shown that a stochastic EM field with Gaussian probability distribution can be completely described by the correlation functions or correlation spectra of all field components [12], [13]. To establish these correlation functions by measurements, the field values have to be measured in all pairs of sampling points and the field values have to be correlated for each pair of sampling points of a defined virtual grid. Due to the equivalence principle and the uniqueness theorem [14], the evolution of the correlation functions for the EM field propagating into the environment can be computed by analyzing data from near-field two-point measurements of the tangential electric and/or magnetic field components in a surface enclosing the interferer [15]-[22].

In the far-field region, within a certain coherence area, the EM field exhibits transverse coherence also when originating from incoherent sources [23]. Therefore, within the coherence area only one reference probe needs to be positioned. Different from this, in the general case a complete experimental near-field characterization providing all necessary information for the computation of the energy density distribution in complex environments requires sampling of the EM field with at least two field probes in order to measure also the cross correlations of the field components sensed at the different field points [12], [13], [24]-[26]. The two-point correlation field measurement and analysis methods were discussed for cyclostationary EM fields in [27], [28].

Figure 1 shows the schematic of a two-point scanner used for measuring and recording the near-field correlation of stochastic EM fields [12]. Two electric or magnetic field probes are used to scan the respective near-field simultaneously. The measured signals are amplified and digitized and the auto- and cross-correlation functions are computed in the central processing and control unit, which also controls the positioning of the two probes.

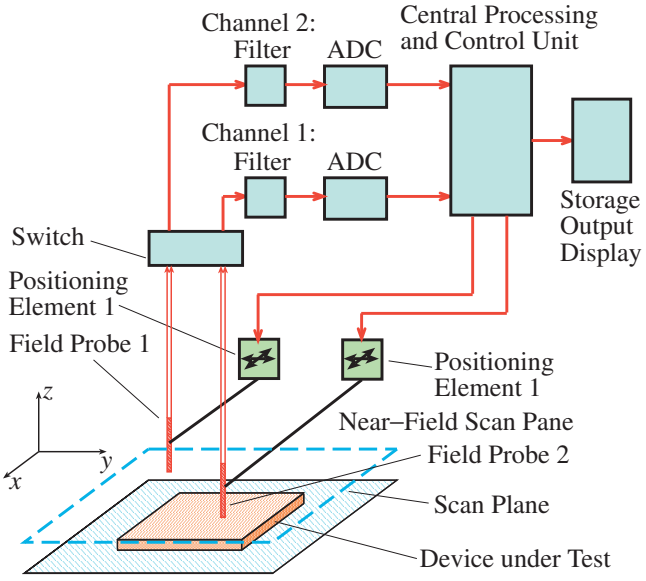

Figure 1. Schematic drawing of the near-field scanning system.

The time-domain correlation dyadics of two electric field variables $\boldsymbol{E}(x_1, t_1)$ and $\boldsymbol{E}(x_2, t_2)$ measured at points $\boldsymbol{x}_1$ and $\boldsymbol{x}_2$, at times t_1 and t_2, respectively are given by

$$\Gamma_E\left(\boldsymbol{x}_1,\boldsymbol{x}_2,t_1,t_2\right)=\left\langle \boldsymbol{E}\left(\boldsymbol{x}_1,t_1\right)\boldsymbol{E}^{\dagger}\left(\boldsymbol{x}_2,t_2\right)\right\rangle \quad (1)$$

$$\Gamma_H\left(\boldsymbol{x}_1,\boldsymbol{x}_2,t_1,t_2\right)=\left\langle \boldsymbol{H}\left(\boldsymbol{x}_1,t_1\right)\boldsymbol{H}^{\dagger}\left(\boldsymbol{x}_2,t_2\right)\right\rangle \quad (2)$$

where $\boldsymbol{E}(\boldsymbol{x}, t)$ and $\boldsymbol{H}(\boldsymbol{x}, t)$ are the electric and magnetic field vectors, and the symbol † denotes the Hermitian conjugate which is equivalent to the transpose of the vector for our real valued time domain field vectors [27], [28]. For $\boldsymbol{x}_1 = \boldsymbol{x}_2$ this function is the autocorrelation function of the field and for $\boldsymbol{x}_1 \neq \boldsymbol{x}_2$ it is the cross-correlation function relating the field amplitudes at the points $\boldsymbol{x}_1$ and $\boldsymbol{x}_2$ [12], [13]. Two-point sampling yields an enormous amount of information since the $2n$ field components sampled at n sampling points yield a total of $2n$ autocorrelation signals plus $n(2n\text{-}1)$ cross correlation signals. The existing near-field correlations allow a considerable reduction of the amount of sampling reference

points. An efficient method for the reduction of reference points is the principal component analysis (PCA) for eigenvalue decomposition of the correlation matrix [29], [30]. Applying this method allows the reduction of the reference probe positions down to the number of principal eigenvalues. The number of applied principal eigenvalues determines the accuracy of the obtained data.

Time-domain EM interference measurement systems sample the EMI signal with gigahertz sampling rates and can be used for computing the EMI spectrum by fast Fourier transform (FFT) and reduce the measurement time compared with conventional EMI receivers by up to five orders of magnitude [31]-[35]. Exploiting the cyclostationary characteristics of stochastic fields greatly simplifies the analysis of stochastic EM fields. Time domain measurement systems allow the characterization of the stochastic field with a single measurement run in a wide frequency band. Time-domain methods are also advantageous for modeling of EM fields [36], [37].

The important feature provided by the statistical cyclic averaging procedure is the capability to distinguish cyclostationary signals from a mixture of stochastic processes such as stationary noise with deterministic signals and even from other cyclostationary signals with distinct cyclic frequencies. Spatial localization of the distributed radiating sources on the surface of PCB in conjunction with their average power characteristics and the time domain distribution of the autocorrelation characteristics of the EM field governed by a stochastic process with predefined cyclostationary properties [38] can be used for the prediction of regions exhibiting significant average EM power levels on the surface of the PCB and in the environment of the ED within its enclosure [39]. The quantitative characterization of crosstalk and coupling between transmission lines carrying the data sequences, and subsequent estimation of BER caused by the crosstalk can be implemented using their cyclostationary properties.

Time domain methods are efficient for modeling the propagation of stochastic EM fields based on measured time domain data. In [24], [25] a detailed treatment of modeling of noisy electromagnetic fields excited by electric and/or magnetic polarizations as well as formulations for its numerical implementation along with numerical and experimental based examples for the method were presented. Near-field to far-field propagation based on measurement data using Jefimenko's equations is considered in [40], [41]. Different from [24], [25] where the integral relations were established on the basis of the electric and/or magnetic Hertzian vector it was presented a formulation for computing the field dyadics based on Jefimenko's equations [42]-[45] in which the magnetic vector potential and the electric charge are used in the integral relations.

The characterization of near-field EM emissions from the PCB of an ED can be implemented in frequency or in time domain. Frequency domain characteristics may be obtained by spectrum analyzers connected to the near-field probes installed into the scanning system [46] or clustered within the array for quantification of the emitted power spectrum from the device under test (DUT) [47]-[50]. Such characterization is useful for registration of the average power for periodic deterministic or stationary stochastic radiations from the DUT. Time-domain measurement equipment is based on a real time digital multi-channel oscilloscope in conjunction with the sequential scanning system including near-field probes [26], [51], [52]. The oscilloscope is used for the registration of the waveforms provided by two near-field probes. The subsequent digital processing of the stored sequences can be used for the appropriate averaging and extraction of the information associated with the functioning of the DUT. For implementing the cyclic averaging of the registered signals in each scanning point the bit rate needs to be known exactly. It can be evaluated for each scanning point separately by estimating the power spectrum of the registered signal revealing the presence of harmonics with frequencies multiple to the fundamental frequency of the periodic deterministic component existing in the registered signal [53], [54]. The estimated fundamental frequency can be used for cyclic averaging of registered data. The results of the time domain approach for the cyclostationary characterization presented in [8], [55] show the possibility for extraction of cyclostationary parameters from generated data sequences.

A quantitative analysis of the hidden cyclostationary properties of the random non-periodic data sequences associated with the regular shape of the single symbol pulse is performed in [56]. The analysis allows an implementation of spatial time localization of radiated sources exhibiting predefined cyclostationary properties of its two-dimensional auto covariance function. The hidden properties of the data sequences are masked by the deterministic periodic clock signals accompanying the random cyclostationary process. The cyclic averaging of the measured signal can reveal its correlation properties. If the stationary noise and some other stochastic or deterministic periodic signals with different periods exist in the mixture composing a realization of investigating random process, it will not change the shape of the estimated two-dimensional auto covariance function over the time axis. This effect allows selecting random signals with predefined cyclostationary properties from other signals in the surrounding of the PCB such as data random sequences with different bit rates, deterministic clock signals and stationary noise. The procedure of cyclostationary sources localization allows to investigate the extracted sources separately. The obtained space-time near-field distributions of the cyclostationary characteristics of the averaged power can be used for the prediction of its values in any point of the space surrounding the PCB [25], and consequently evaluate the possible impact on the nearby EDs. It is known from [57] that the crosstalk and coupling between transmission lines carrying the data sequences with similar cyclostationary properties leads to a substantial increase of the BER of the communication link.

This paper presents an approach for quantifying emissions and coupling of stochastic fields using their cyclostationary properties. Following this introduction, a brief theoretical description of time domain characteristics for cyclostationary stochastic processes for modeling data sequences flowing along transmission lines of the ED will be given. The measurement techniques and necessary instrumentation for near-field data acquisition of the EM radiations from the ED will be described in the subsequent section. Experimental spatial localization of distributed radiating sources with

cyclic properties will be demonstrated. Spatial separation of EMI sources with different cyclic frequencies revealing the actual positions of the transmission lines between different blocks on the surface of the PCB with corresponding average power distributions will be presented. Next application describes the quantitative characterization of crosstalk and coupling between transmission lines carrying the data sequences by using their cyclostationary characteristics, which allows to estimate BER of the communication links. The discussion on further development of this approach considering stochastics for improving electromagnetic compatibility and signal integrity of the emerging high-speed miniature EDs will conclude the paper.

II. Theory of Cyclostationarity

The reliable data transferring between blocks of the ED is realized by coding of the logical bits into voltage or current signals. The physical signals propagating along the transmission lines may cause EM emissions, which can be sensed by near-field probes scanning the area above the surface of the PCB. The obtained signal is modelled by a cyclostationary random process (CSRP) with periodically repeating characteristics. The period of these characteristics is called a cycle and is equal to the single symbol duration T of the data sequence.

Consider the signal $s(t)$, obtained by the near-field probe measuring a component of the EM field at a single scanning point and registered by the real-time digital oscilloscope. As shown in Fig. 2 this signal consists of the environmental noise $w(t)$, deterministic or random nonstationary signals $d(t)$ and observable data transferring signal with cyclostationary behavior $x(t)$:

$$s(t) = x(t) + d(t) + w(t) \tag{3}$$

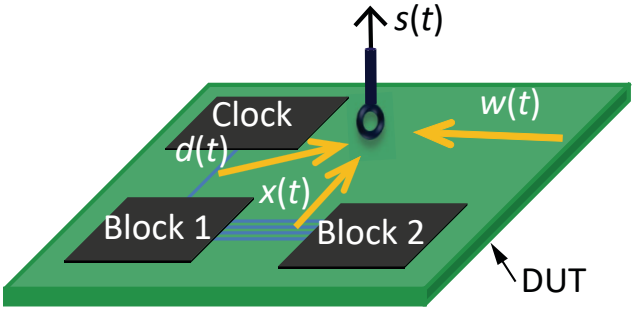

Figure 2. Components of the near-field measured signal.

For extraction of the cyclostationary signal from the mixture of received signals, the statistical averaging assuming the known cyclic frequency $\alpha = 1/T$ of the CSRP can be applied. The canonical averaging using a joint cumulative probability distribution [58] is not applicable due to the presence of unpredictable disturbances during the measurements. Moreover, the necessary probability distribution is not always available, but the statistical cyclic ensemble averaging of the measured random signal $s(t)$ allows not only the extraction but also the quantitative characterization of the emissions $x(t)$ caused by data transferring stochastic sequences.

The probabilistic model of the continuous-time CSRP $X(t)$ formed by stochastic sequences $x(t)$ can be described by appropriate transformations of the initial discrete-time random process $A[k]$ corresponding to the binary information prepared for transferring between Block 1 and Block 2 shown in Fig. 2 [38]. For simplicity reasons the random process $A[k]$ can be defined as a sequence of mutually independent Bernoulli random variables $A[k] = \{a_0 = 0, a_1 = -1\}$ with the probability distribution $P_A(a) = p\delta[a - a_1] + (1 - p)\delta[a - a_0]$, where p is a probability of a_1.

The physical signal $v(t)$ propagating along the transmission lines between Block 1 and Block 2 is generated by an analog device forming rising and falling edges of the signal $v(t)$. It can be represented by a stochastic process $V(t)$ defined as follows:

$$V(t) = \sum_{n=-\infty}^{\infty} U_k \cdot \phi_{\text{rise}}(t - kT) + D_k \cdot \psi_{\text{fall}}(t - kT) \tag{4}$$

where $\phi_{\text{rise}}(t)$ and $\psi_{\text{fall}}(t)$ are one-sided deterministic functions with infinite duration describing rising and falling edges of the signal $v(t)$ shown in Fig. 3. Values of random variables U_k and D_k are defined by the previous value of the random variable A_k as follows:

$$U_k = \begin{cases} 1, \text{ if } A_k > A_{k-1} \\ 0, \text{ if } A_k \le A_{k-1} \end{cases} \tag{5a}$$

$$D_k = \begin{cases} 1, \text{ if } A_k < A_{k-1} \\ 0, \text{ if } A_k \ge A_{k-1} \end{cases} \tag{5b}$$

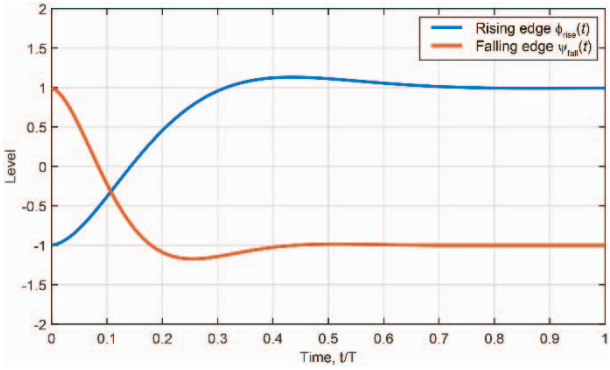

Figure 3. Rising edge and falling edge of the signal v(t).

The model of the cyclostationary process $V(t)$ allows us to assign the shapes of rising and falling edges of the random signal in the transmission line separately. Such a model describes practical observations of transmission line signals demonstrating different shapes of rising and falling edges. This can be explained by the presence of two separate circuits forming rising and falling edges of the signal. Probabilities of random variables U_k and D_k can be defined from (5a) and (5b) as marginal probability distributions $P_U(u)$ and $P_D(d)$ of the joint random variable (UD) as follows:

$$P_U(u) = (1 - p + p^2)\delta[u] + (1 - p)\, p\delta[u - 1] \tag{6a}$$

$$P_D(d) = (1 - p + p^2)\delta[d] + (1 - p)\, p\delta[d - 1] \tag{6b}$$

The physical signal $v(t)$ moving along the transmission line can be viewed as a source of the radiating EM field preserving cyclostationary properties of the source signal. The relation between the signal $x(t)$ at the output of the scanning near-field probe and its source signal $v(t)$ can be represented by the convolution with the impulse response $h(t)$ of the unknown linear dynamical system connecting these two signals:

$$x(t) = v(t) * h(t) = \int_0^t h(\tau)v(t-\tau)d\tau \qquad (7)$$

The procedure for extraction of the impulse response of the linear dynamical system including near-field probes is described in [51]. The stochastic signal $x(t)$ can be modeled as a random process $X(t)$ exhibiting cyclostationary properties due to the periodical nature and the predefined bit rate of the signal $v(t)$. The stochastic process $X(t)$ involves two deterministic pulses with the probability characteristics inherited from initial random process $V(t)$:

$$X(t) = \sum_{k=-\infty}^{\infty} U_k \gamma_{\text{rise}}(t-kT) + D_k \gamma_{\text{fall}}(t-kT) \qquad (8)$$

where $\gamma_{\text{rise}}(t)$ and $\gamma_{\text{fall}}(t)$ are impulse functions describing the linear transformation of rising and falling edges of the signal $v(t)$, shown in Fig. 4.

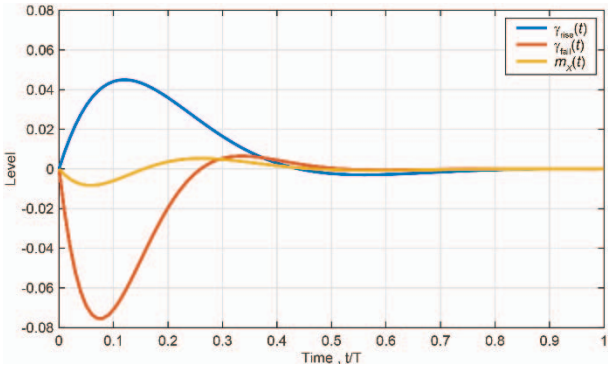

Figure 4. Impulse functions of rising edge, falling edge and expectation function of the signal x(t).

The presented probabilistic model of the CSRP $X(t)$ allows to evaluate periodic cyclostationary characteristics of the process. Periodic expectation function $m_X(t)$ of the cyclostationary random process $X(t)$ can be defined by canonical probabilistic averaging of (8) during the period T, defined by the known bit rate of the signal $v(t)$ [7]. Applying the linearity property of the expectation operator $E\{\cdot\}$ the expectation function of the CSRP can be defined as follows:

$$\begin{aligned} m_X(t) &= E\{X(t)\} = E\{U_k\}\gamma_{\text{rise}}(t) + E\{D_k\}\gamma_{\text{fall}}(t) \\ &= p(1-p)[\gamma_{\text{rise}}(t) + \gamma_{\text{fall}}(t)] \end{aligned} \qquad (9)$$

An example of the periodic expectation function $m_X(t)$ for $p = 1/2$ is shown in Fig. 4.

The two-dimensional periodic autocorrelation function $R_X(t, \tau)$ of the CSRP $X(t)$ can be defined by the expectation operator applied to the product of two symmetrically shifted at $\pm\tau/2$ random processes (8) assuming (6) shown below in (10).

The cross-section of $R_X(t, \tau)$ for $\tau = 0$ represents the periodic instantaneous average power of the CSRP $X(t)$:

$$R_X(t,0) = E\{X^2(t)\} = p_X(t) \qquad (11)$$

The periodic autocorrelation function $R_X(t, \tau)$ of the CSRP $X(t)$ and its sections are shown in Fig. 5.

Another second order characteristic of the CSRP $X(t)$ is a cyclic autocorrelation function (CACF) $C_X^{\alpha}(k, \tau)$. CACF defines depending amplitudes and phases for complex exponential functions of multiple cyclic frequencies $F_k = k\alpha = k/T$ on time shift τ. Due to the periodicity of autocorrelation function $R_X(t, \tau)$ along the time axis t, CACF is discrete over frequency axis with nonzero "walls" at discrete frequencies F_k. Each "wall" of the CACF is a complex continuous function along the time-shift axis τ. CACF can be evaluated by applying Fourier series expansion to the periodic autocorrelation function $R_X(t, \tau)$:

$$R_X(t,\tau) = \sum_{k=-K}^{K} C_X^{\alpha}(k,\tau)\cdot e^{j2\pi k\alpha t} \qquad (12a)$$

$$C_X^{\alpha}(k,\tau) = \frac{1}{T}\int_0^T R_X(t,\tau)\cdot e^{-j2\pi k\alpha t}dt \qquad (12b)$$

The value of the CACF for $\tau = 0$ and $k = 0$ represents the average power of the CSRP $X(t)$:

$$C_X^{\alpha}(0,0) = \frac{1}{T}\int_0^T p_X(t)dt = P_X \qquad (13)$$

The magnitude of the CACF of the CSRP $X(t)$ is shown in Fig. 6.

$$\begin{aligned} R_X(t,\tau) = E\left\{X\left(t+\frac{\tau}{2}\right)X\left(t-\frac{\tau}{2}\right)\right\} &= p(1-p)\cdot\left[\gamma_{\text{rise}}\left(t+\frac{\tau}{2}\right)\gamma_{\text{rise}}\left(t-\frac{\tau}{2}\right)+\gamma_{\text{fall}}\left(t+\frac{\tau}{2}\right)\gamma_{\text{fall}}\left(t-\frac{\tau}{2}\right)\right. \\ &+p\cdot\gamma_{\text{rise}}\left(t+\frac{\tau}{2}\right)\gamma_{\text{fall}}\left(t-T-\frac{\tau}{2}\right)+p\cdot\gamma_{\text{rise}}\left(t-\frac{\tau}{2}\right)\gamma_{\text{fall}}\left(t-T+\frac{\tau}{2}\right) \\ &\left.+(1-p)\cdot\gamma_{\text{rise}}\left(t-T-\frac{\tau}{2}\right)\gamma_{\text{fall}}\left(t+\frac{\tau}{2}\right)+(1-p)\cdot\gamma_{\text{rise}}\left(t-T+\frac{\tau}{2}\right)\gamma_{\text{fall}}\left(t-\frac{\tau}{2}\right)\right] \end{aligned} \qquad (10)$$

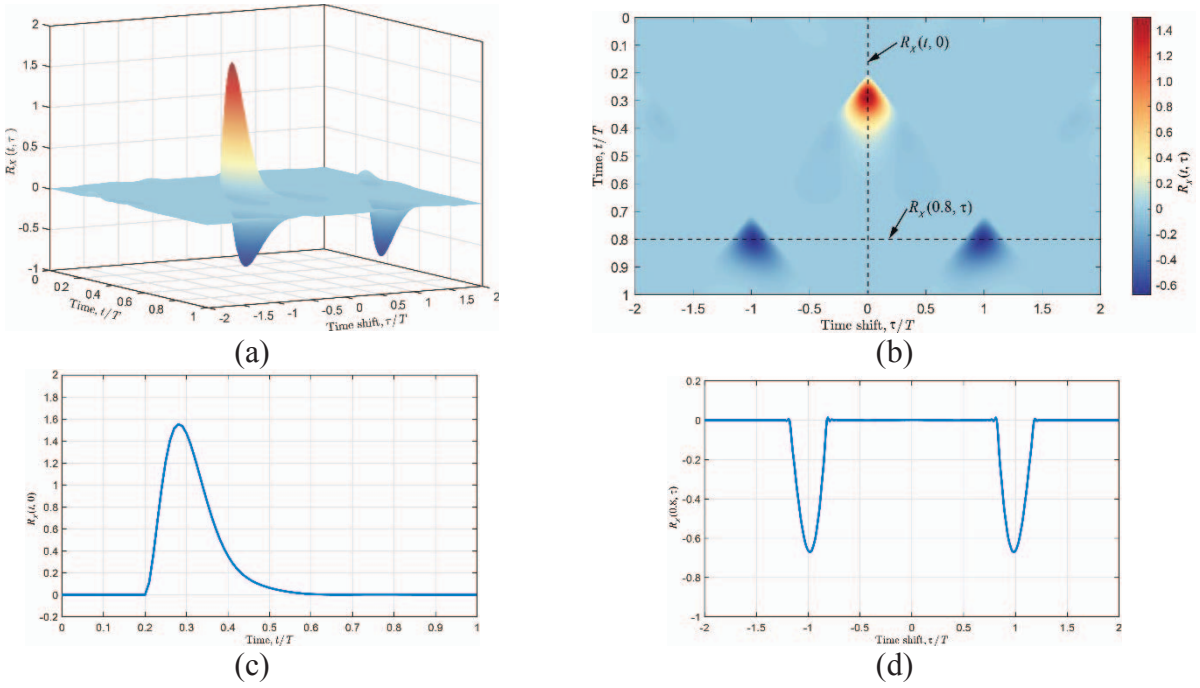

Figure 5. Periodic autocorrelation function of the CSRP X(t) (a, b) and its sections for τ = 0 (c) and t = t – 0.8T (d).

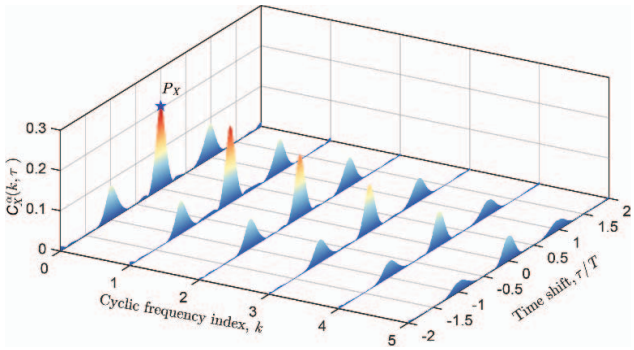

Figure 6. Magnitude of the CACF of the CSRP X(t).

If periodic expectation function $m_X(t)$ of the CSRP $X(t)$ is nonzero, it can mask the dependence of the variance of CSRP on time and time shift. To reveal this hidden cyclostationary property of the random process the expectation function $m_X(t)$ needs to be properly extracted from the process $X(t)$ itself or from its evaluated autocorrelation characteristics.

The two-dimensional periodic auto covariance function $Cov_X(t,\tau)$ of the random process $X(t)$ is evaluated by subtraction of the product of two symmetrically shifted at ±τ/2 expectation functions $m_X(t)$ as follows:

$$Cov_X(t,\tau) = R_X(t,\tau) - m_X\left(t+\frac{\tau}{2}\right)\cdot m_X\left(t-\frac{\tau}{2}\right) \quad (14)$$

The obtained periodic auto covariance function can be used in (12b) for evaluation of cyclic auto covariance function $Cov_x^{\alpha}(k, \tau)$. Its value for τ = 0 and k = 0 represents the average power of the residue CSRP $X_r(t) = X(t) - m_X(t)$ with zero expectation function:

$$Cov_X^{\alpha}(0,0) = \frac{1}{T}\int_0^T E\{X_r^2(t)\}dt = P_{X_r} \quad (15)$$

Another way for evaluation of the cyclostationary characteristics of the signal with cyclostationary behavior $x(t)$ is the *statistical cyclic averaging* of the sufficiently long realization of the measured signal $s(t)$ in time domain. The important advantage of the statistical cyclic averaging procedure of the random signal with known cyclic frequency $\alpha = 1/T$ is its immunity to the stationary noises $w(t)$, deterministic or random nonstationary signals $d(t)$ and even to other cyclostationary signals with distinct cyclic frequencies [59]. The existence of signals $d(t)$ and $w(t)$ in the measured signal (3) leads to an increase of the constant component of the periodic instantaneous average power (11) of the measured signal and does not affect its shape.

The periodic sample mean function $\mu_x(t)$ of the measured cyclostationary component $x(t)$ of the signal (3) is given by

$$\mu_x(t) = \langle x(t)\rangle = \lim_{N\to\infty}\frac{1}{2N+1}\sum_{n=-N}^{N} x(t-nT) \quad (16)$$

If the evaluated sample mean function $\mu_x(t)$ coincides with periodic expectation function $m_X(t)$, the stochastic process $X(t)$ possesses the first order cycloergodic property. It means that statistical cyclic averaging <□> of the random signal $x(t)$ gives the same result as probabilistic ensemble averaging $E\{\cdot\}$ of the stochastic process $X(t)$.

Statistical cyclic averaging of the product of two symmetrically shifted at ±τ/2 measured cyclostationary components $x(t)$ gives the estimation of periodic autocorrelation function, which can be expanded into the Fourier series for evaluation of the cyclic autocorrelation function $c_x^{\alpha}(k, \tau)$:

$$r_x(t,\tau) = \left\langle x\left(t+\frac{\tau}{2}\right)x\left(t-\frac{\tau}{2}\right)\right\rangle = \sum_{k=-K}^{K} c_x^{\alpha}(k,\tau)\cdot e^{j2\pi k\alpha t} \quad (17)$$

Each component of cyclic autocorrelation function can be statistically estimated by time domain averaging of the non-linear time-shift transformation of the $x(t)$ as follows:

$$c_x^{\alpha}(k,\tau) = \lim_{L\to\infty} \frac{1}{L} \int_{-L/2}^{L/2} x\left(t+\frac{\tau}{2}\right) x\left(t-\frac{\tau}{2}\right) \cdot \mathrm{e}^{-j2\pi k\alpha t} dt \qquad (18)$$

where L is the length of the measured realization $x(t)$ in time domain.

The appropriate synchronous subtraction of the periodic sample mean function from the measured signal gives the residual signals $x_r(t) = x(t) - \mu_x(t)$. The periodic auto covariance function can be estimated after the averaging of the residual signals as follows:

$$c_{x_r}(t,\tau) = \left\langle x_r\left(t+\frac{\tau}{2}\right) x_r\left(t-\frac{\tau}{2}\right) \right\rangle \qquad (19)$$

Statistical evaluation of the periodic cross-correlation functions between the signals synchronously measured at some reference point $x_{ref}(t)$ on the surface of the PCB and at the i-th scanning point in the plane over the PCB $x_i(t)$ can be implemented as follows:

$$\begin{aligned} r_{x_i,x_{ref}}(t,\tau) &= \left\langle x_i\left(t+\frac{\tau}{2}\right) x_{ref}\left(t-\frac{\tau}{2}\right) \right\rangle \\ &= \sum_{k=-K}^{K} c_{x_i,x_{ref}}^{\alpha}(k,\tau) \cdot \mathrm{e}^{j2\pi k\alpha t} \end{aligned} \qquad (20)$$

Estimated periodic cross-correlation functions can be used for spatial-time characterization of the near field caused by the data transferring along transmission lines of the ED [56]. Another possible application of the periodic cross-correlation functions is the prediction of the angular distribution of the radiated EM field exhibiting the cyclic properties in the surrounding of the PCB. The correlations of the EM field can be obtained by analyzing the cross-correlation characteristics between the signals measured in the far field by receiving antenna and a reference point on the surface the PCB [41], [60].

The statistical cyclic averaging procedure of signals measured by the near-field probe over the surface of the PCB allows us to implement the experimental spatial localization of distributed radiating sources with specified cyclic frequencies. This procedure also will be applied to the spatial separation of EMI sources with different cyclic frequencies and for the quantitative characterization of crosstalk between transmission lines carrying the data sequences, which allows an estimation of the BER of the communication links.

III. Experimental Setup

The measurement setup for time-domain analysis of the cyclostationary properties of the EM emissions from a PCB is shown in Fig. 7. It comprises of the positioning system with scanning near-field probe fixed to the moving scanner head. The positioning system is controlled by special software installed on data acquisition and positioning control computer. The scanning near-field probe and a suitably allocated reference probe are connected through the corresponding preamplifiers to the inputs of the digital oscilloscope for simultaneous and synchronous sampling and registering of the measured signals. The registered data from the oscilloscope is being transferred to the data acquisition computer via Gigabit LAN. Optionally the reference signal can be obtained straight from DUT and connected to the separate input of the digital oscilloscope.

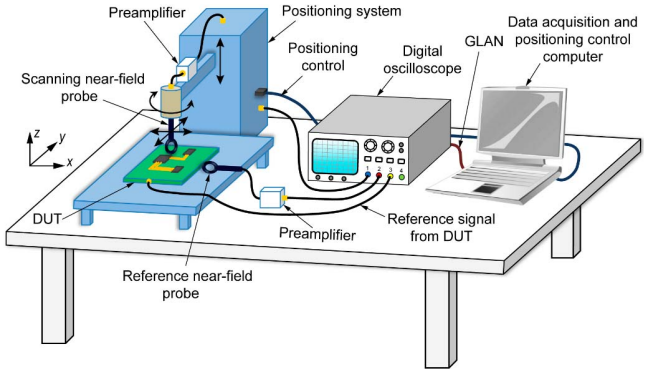

Figure 7. Measurement setup.

It shall be mentioned that the technical specification [61] provides a test procedure for the near electric, magnetic or EM field measurements in close vicinity to the surface of an integrated circuit (IC) with a similar measurement setup albeit without multi-channel time domain characterization and correlation analysis. The specified method provides a mapping of the electric or magnetic near-field emissions to the surface above the IC or PCB of the DUT [62], [63].

The resolution of the measurement is determined by the capability of the measurement probe and the precision of the probe-positioning system. Each scan over a PCB collects a large amount of data depending on the sampling frequency, the number of samples and the number of repeated measurements at each location. This method also requires an analysis and handling of a large amount of data typically performed by dedicated software programs.

The spatial resolution depends on the physical dimensions and construction of the near-field probe. The altitude of the probe above the PCB surface should be chosen in accordance with the PCB configuration. The step size of the probe position shall be chosen to fully utilize the spatial resolution while minimizing the number of measurement points. Step size can be smaller for higher resolution. The scanner position accuracy should be at least 1/10th of the smallest probe size. For time-domain measurements the sampling frequency, triggering conditions, sweep time, etc. need to be adjusted to obtain the desired accuracies and measurement time. The sweep time should be much greater than the PCB operating cycle time, in order to ensure the capture of all expected events (pulses, bursts, etc.).

In case of a probe which measures a single field component only, the probe may be rotated automatically at each sampling location to allow measurement of, for example, the x-directed field component and the y-directed field component, both of which are tangential field components to the scanning plane. If the rotation is manual, it is usual to scan the entire surface with the probe in one

position first and to turn it then by 90° before rescanning the surface. Because of the required precision and repeatability of the measurement results, the probe rotation should be performed very accurately.

The data acquisition system stores the signals measured at the near-field probe output at each location and probe orientation. Post-processing can take into account the gains, losses and phase offsets caused by a preamplifier and cables. Probe calibration data can allow conversion from measured signal level to magnetic or electric field strength.

For our measurements in the open laboratory condition, magnetic field probes from Langer EMV-Technik are used, which are connected to a LeCroy 13 GHz Serial Data Analyzer trough Langer EMV-Technik amplifiers. A desktop PC is used to control the movement of the scanning probe and collect data from the oscilloscope. The fixed reference probe was installed in near vicinity of the data signal source, allowing the moving probe to scan a predefined area on the surface of the PCB. The measured reference signal was registered synchronously with the signal of scanning probe by the digital oscilloscope for further data postprocessing on a separate computer.

IV. Experimental Results

A. Sources Localization

A photo of the experimental setup for the estimation of the spatial source distribution of the EM radiations is shown in Fig. 8. The parameters of the setup are summarized in Table 1, denoted as Experiment 1. The Atlys Spartan-6 training board [64] was used as DUT, which was programmed for sending random digital bit sequence from an FPGA via a strip line to a light-emitting diode (LED) along the strip line. The physical signal formed by this bit sequence was the source of the radiated EMI. The duration of the single bit symbol was chosen $T = 3$ ns.

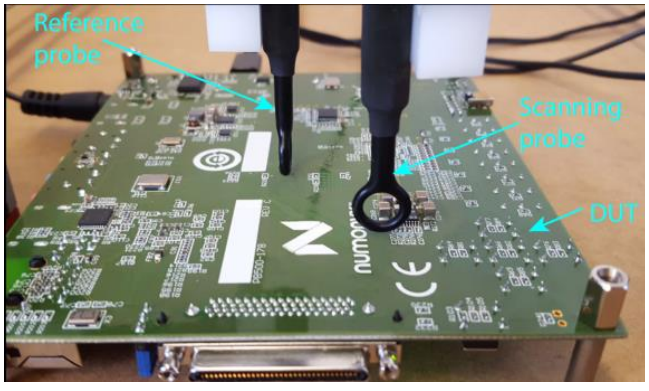

Figure 8. Photo of the experimental setup.

The localization of the transmission line connecting the output of FPGA with the LED in the periphery of the PCB based on EM near-field scanning was implemented by statistical evaluation of the two-dimensional periodic autocorrelation function (17) for $\tau = 0$ at all scanning points over the DUT:

$$r_x(t,0) = \left\langle x^2(t) \right\rangle = P_{x_r}(t) \tag{21}$$

The cross-section of the periodic autocorrelation function (21) represents the dependence of the periodic instantaneous average power of the cyclostationary component $x(t)$ of the measured signal $s(t)$ in the scanning point. The spatial distribution of synchronized evaluated instantaneous average powers for different time moments are shown in Fig. 9. It can be seen how and where the emitted magnetic field corresponding to the surface electric currents of the strip line is moving over the surface of the PCB.

Table 1. Parameters of the experimental setup.

Parameter	Experiment 1	Experiment 2
Scanning step	5 mm	2 mm
Scanning area	110 x 95 mm	72 x 48 mm
High	2 mm	2 mm
Near-field probe	Langer RF-R 50-1	Langer RF-B 3-2
Sampling frequency	40 GSa/s	10 GSa/s
Number of samples	5 M	5 M

In this experiment time synchronization of the measured sequences at each scanning point was implemented by simultaneous registering of signals of reference and scanning probes. During the postprocessing procedure all evaluated similar instantaneous average powers of the reference signal were time shifted into the common location, which resulted in synchronization of autocorrelation functions in all scanning points.

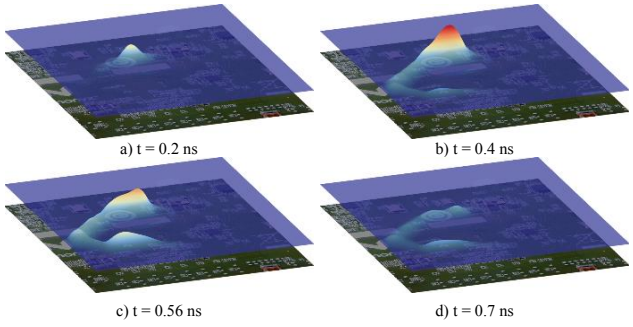

Figure 9. Spatial distribution of instantaneous average powers for different time moments.

B. Separation of Two Sources

A photo of the experimental setup for source localization and source separation, estimating the spatial near-field distributions for EMI originating from transmission lines carrying digital bit signals with different bit rates, is presented in Fig. 10.

The parameters for this setup are given are given in Table 1, denoted as Experiment 2. A development board with a Xilinx FPGA Artix 7 was programmed for simultaneously sending two random bit sequences with different bit rates to the predefined outputs on the surface of the PCB. The traces of differential strip lines transferring random bit sequences are shown schematically on the

photo of the PCB surface in Fig. 11. The bit rates for two random sequences were chosen as 100 MHz and 130 MHz respectively. For the near-field measurements, scanning points were defined inside the depicted scanning area on a rectangular mesh as defined in Table 1. The reference probe was placed on the other side of the PCB near the point where the observed signal reveals the superposition of both signals emitted by random sequences.

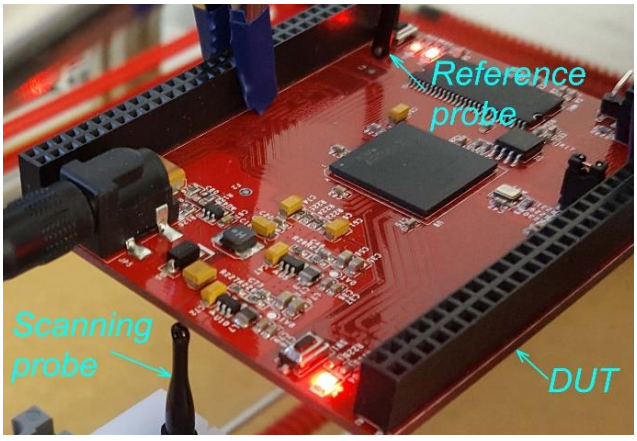

Figure 10. Photo of the experimental setup.

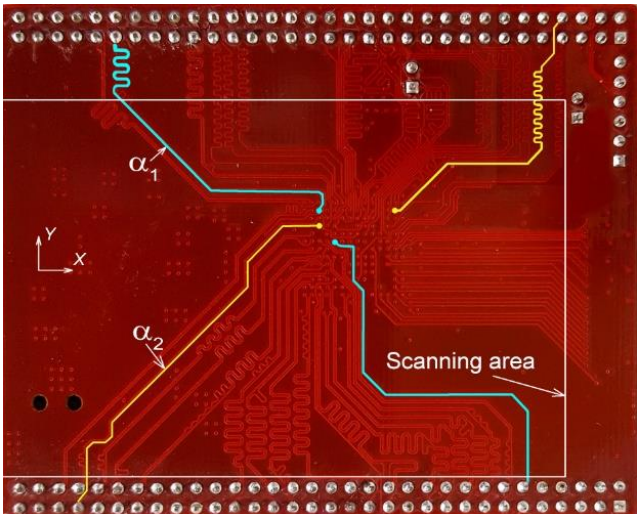

Figure 11. Device under test.

Results of nonsynchronous averaging for measured squared signals at each scanning point yield the spatial diagram of the mean power distribution of the EMI in the near field of the DUT. This distribution is depicted in Fig. 12. In this diagram the so-called hot spots on the surface of the PCB can be seen corresponding to the mean power of EM emissions caused by the random bit sequences with different bit rates propagating along the differential strip lines going from the FPGA to the corresponding outputs.

To separate the detected emissions in accordance with different bit rates of digital data sequences, the statistical averaging procedure was implemented. After application of the averaging algorithms for two cycle frequencies α_1 = 100 MHz and α_2 = 130 MHz in accordance with (19) the periodic auto covariance functions $c_{x_1}(t, \tau)$ and $c_{x_2}(t, \tau)$ were obtained for each point at the scanning plane.

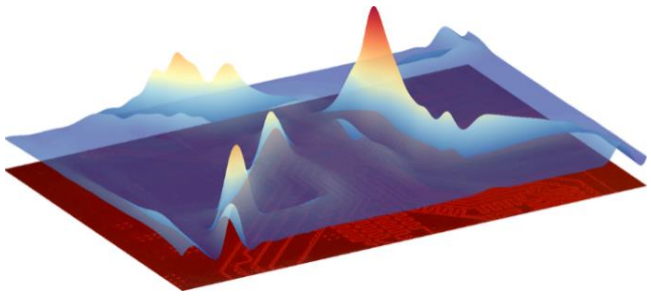

Figure 12. Mean power of EMI in the near field of the DUT.

The synchronization of all periodic auto covariance functions can be implemented using the reference signal synchronously registered by the real-time digital oscilloscope simultaneously with the EM near-field scanning signal during the measurement of the near-field emission from the PCB. This allows us to realize the time evolution experiment for each digital signal, just like in Experiment 1. Maximum values of periodic auto covariance function visualized for the scanning plane are given in Fig. 13 and show good separation of two transmission lines.

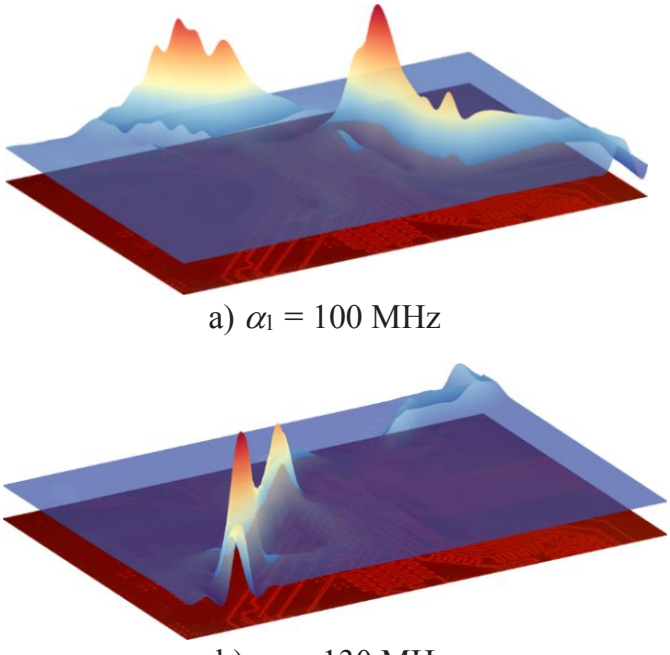

a) α_1 = 100 MHz

b) α_2 = 130 MHz

Figure 13. Spatial distribution of the two-dimensional auto covariance functions maximums.

The presented spatial distributions of the statistically evaluated cyclic characteristics resemble the geometric configuration of the transmission strip lines shown in Fig. 11. We conclude that the cyclic averaging with the known cyclic frequency allows extract the spatial distribution of the EM radiation sources with the defined cyclostationary properties.

C. Characterization of Crosstalk Between Transmission Lines

The purpose of the third experiment was to clarify the properties of the noise corrupting the information bearing signal when

transmitted along the transmission line. For this, a pseudorandom digital sequence has been generated and transmitted along the manufactured strip line matched with the generator and oscilloscope in the wide frequency bandwidth up to 3 GHz. The manufactured transmission line and the experiment setup are shown in Fig. 14. The binary pseudo random bit sequences (PRBS) were generated by a Xilinx FPGA Artix-7 development board. The length of PRBS with repetition rate F_b = 250 MHz and the values of the symbol levels equal to 0 and 2.15 V was chosen equal 1023 bits. The digital signals are fed to the micro strip lines through coax cables. The micro strip lines were fabricated on a 1.6-mm-thick FR4 substrate with a characteristic impedance of 50 Ω and a length of 50 mm. Width of the micro strip lines with zigzag configuration shown in Fig. 14 (a) is 1.85 mm. One of the strip lines is assumed to be an aggressor emitting the signal corrupting the victim pseudorandom data sequence as shown in Fig. 14 (b). The distance between victim and aggressor circuit boards is h = 1 mm.

The distribution and the value of the aggressor's radiated emissions were measured using a near-field scanning system. The near-field probe was placed over the strip line at the height 1 mm as presented in Fig. 15. The signal transmitted along the aggressor strip line was generated with the same repetition rate, but the pseudorandom sequence had the distinct period from the victim sequence. The eye diagram of the signal in the victim strip line without crosstalk is presented in Fig. 16.

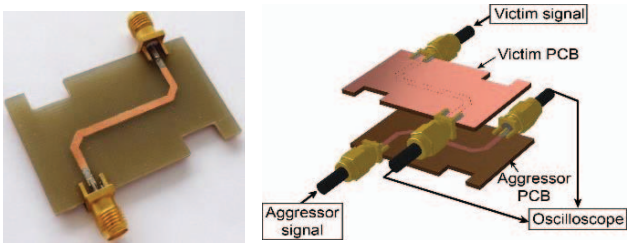

(a) photo of the PCB (b) scheme of the experimental setup

Figure 14. Device under test.

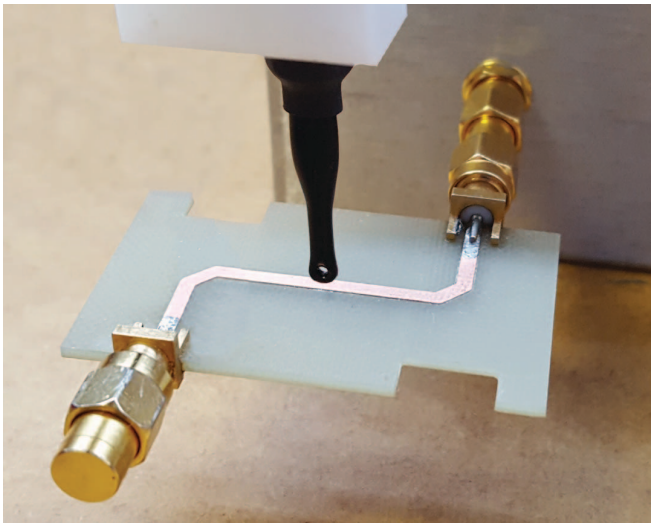

Figure 15. Experiment setup in the near-field measurement.

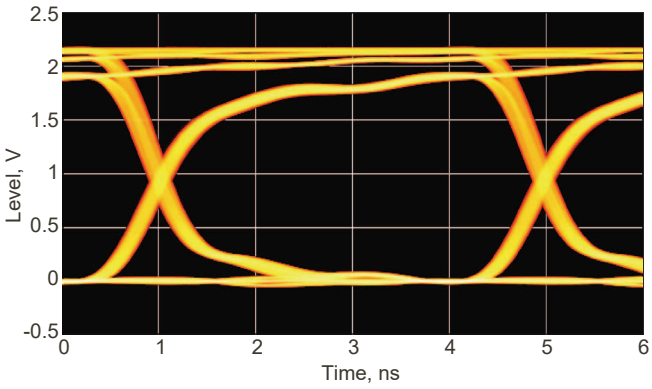

Figure 16. Eye diagram of the signal in the victim strip line without crosstalk.

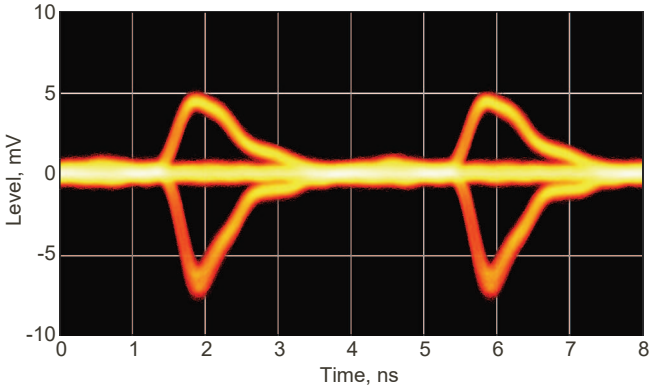

Figure 17. Eye diagram of the signal in the near-field of the strip line.

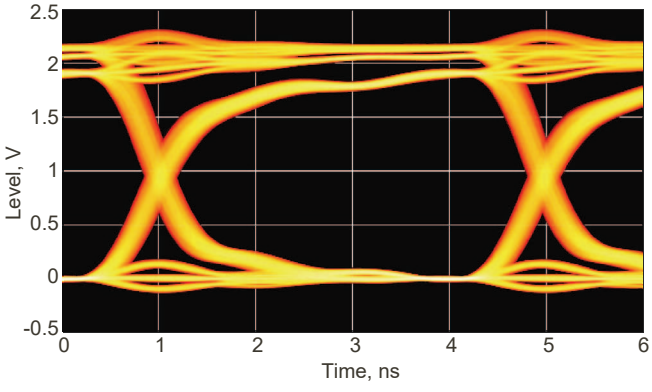

Figure 18. Eye diagram of the victim signal with the mutual crosstalk.

The eye diagram of the aggressor signal measured by the near-field system is shown in Fig. 17. The peaks of this signal correspond to the rising and falling ages of the signal in the strip line. Figure 18 shows the eye diagram of the signal registered by the digital oscilloscope in victim strip line corrupted by the emissions of the interference signal from the aggressor strip line. The widening of the eye's boarders caused by the total digital jitter can be clearly seen including the crosstalk from the aggressor's communication link. The crosstalk between the neighboring circuit boards significantly increases the level of the total jitter including the data depended crosstalk due to the cyclostationary stochastic process.

Statistical cyclic averaging of the measured signal and subsequent excluding of the evaluated sample mean periodic function gives the two-dimensional periodic auto covariance function (19). Estimated average instantaneous power dependencies for duration of one period were obtained from the cross-section of corresponding auto covariance functions for $\tau = 0$. The comparison of two obtained cross sections representing two measured total jitters in the victim transmission line with aggressor crosstalk and the total jitter without crosstalk from the neighboring circuit board is presented in Fig. 19.

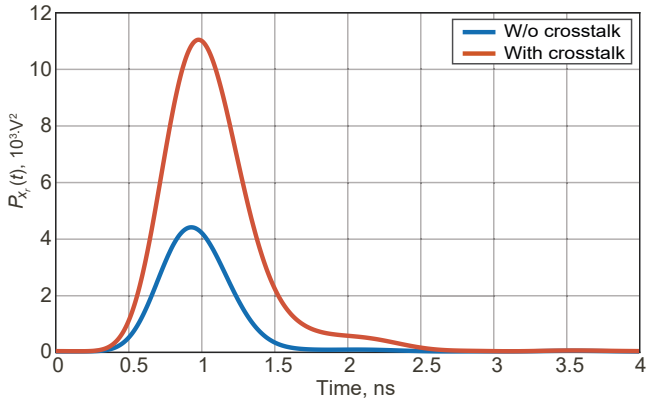

Figure 19. Averaged instantaneous periodic power of the noise in victim line.

The obtained averaged instantaneous periodic power coincides with the variance of the probability density function of the amplitude histograms assembled for each instant of time using the corresponding eye diagram of the transmitted data sequence. The mean values of the defined probability density functions coincide with the values of the averaged periodic sample mean functions $\mu_x(t)$. Eye diagrams can be used for the prediction of the bit error ratio by evaluating the histogram of points crossing the predefined synchronization threshold with subsequent estimation of BER caused by the jitter induced by crosstalk between strip lines as in [65]. Degradation of bit error rate corresponding to histograms due to mutual crosstalk between the lines is shown in Fig. 20.

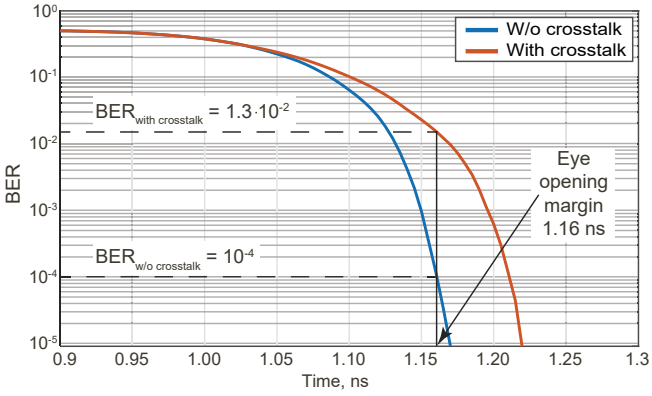

Figure 20. Bit error plot for the victim signal.

The evaluated bit error plot for the victim signal can be prolonged for a reduced BER by assuming the mathematical description of the experimentally evaluated histograms of the crossing points.

V. Conclusion

Increasing complexity and package density of modern digital electronic circuitry triggers the necessity of computer aided design of electronic devices in an early stage of their development. Consideration of EMI caused by high-speed data exchange is of paramount importance. The conventional deterministic approach to the analysis of EMI is not applicable for stochastic fields. The procedure of cyclic averaging applied to the random signals allows to reveal the signals' hidden cyclostationary properties and realize selective quantitative prediction of radiated emissions caused by data streams inside and outside of the enclosure of digital electronic devices.

The probabilistic model of cyclostationary random emissions proposed in this paper predicts the correlation and average power characteristics of the stochastic process for any probability distribution and shape of bit pulses of the digital signals. Statistical cyclic averaging of the measured time domain signals was used for evaluation of cyclostationary characteristics and verification of the probability models. The important feature of the statistical cyclic averaging procedure is its immunity to signals not possessing extracting cyclic properties.

The measurement setup for analysis of EM emissions from PCBs of digital EDs included scanning near-field probes and digital oscilloscope. This system allows simultaneously and synchronously sampling and registering of the emitted EM radiation. After a postprocessing procedure, the spatial localization of distributed radiation sources with specified cyclic frequencies on the surface of the PCB was realized. The proposed cyclic averaging was applied for spatial separation of radiation sources with different bit rates and for the quantitative characterization of crosstalk between transmission lines carrying the data sequences.

The presented experimental investigations resulted in exposure of regions on the surface of the PCB with most powerful cyclostationary components. Such regions need to be excluded from the PCB areas for possible routing through of transmission lines with similar cyclostationary properties for reducing the possible crosstalk and decreasing the BER of communication links. Future research shall provide the prediction of random EM fields with defined cyclic properties in the relative far region from the emitting distributed sources causing harmful interference for other digital devices in the environment of the radiating source.

VI. References

1. H. Boss, "Demystifying signal and power integrity," IEEE Microw. Mag., vol. 12, no. 5, pp. 6–10, August 2011.
2. T.-L. Wu, F. Buesink, and F. Canavero, "Overview of signal integrity and EMC design technologies on PCB: fundamentals and latest progress," IEEE Trans. Electromagn. Compat., vol. 55, no. 4, pp. 624– 638, 2013.
3. S. Wane, O. Doussin, D. Bajon, J. A. Russer, and P. Russer, "Stochastic approach for power integrity, signal integrity, EMC and EMI analysis of moving objects," in Int. Conf. Electromagn. in Adv. Appl. (ICEAA), 2015. IEEE, Sep. 7-11, 2015.
4. S. Wane, D. Bajon, D. Lesénéchal, J. A. Russer, P. Russer, D. Thomas, G. Tan-

ner, G. Gradoni, and Y. Kuznetsov, "Near-field measurement of connected smart RFIC objects accounting for environmental uncertainties," in Proc. 46th Europe Microw. Conf., London, U.K., 3-7 Oct 2016.
5. B. Ravelo and O. Maurice, "Kron-Branin Modeling of Y-Y-Tree Interconnects for the PCB Signal Integrity Analysis," IEEE Trans. Electromagn. Compat., vol. 59, no. 2, pp. 411–419, Apr. 2017.
6. F. Leferink, "Interfered technology: A radiant future: A look forward to EMC in 2023, five years from now," IEEE Electromagnetic Compatibility Magazine, vol. 7, no. 4, pp. 69–75, 2018.
7. A. Gardner, A. Napolitano, and L. Paura, "Cyclostationarity: Half a century of research," Signal Processing, vol. 86, no. 4, pp. 639–697, Apr. 2006.
8. Y. Kuznetsov, A. Baev, M. Konovalyuk, A. Gorbunova, M. Haider, J.A. Russer, P. Russer, "Characterization of the Cyclostationary Emissions in the Near-Field of Electronic Device," in Int. Symp. on Electromagnetic Compatibility – EMC EUROPE, Amsterdam, Netherlands, 27-30 Aug., pp. 573-578, 2018.
9. P.P.J. Schreier and P.L.L. Scharf, "Statistical Signal Processing of Complex-Valued Data: The Theory of Improper and Noncircular Signals", 1st ed. Cambridge, New York: Cambridge University Press, 2010.
10. X. Tong, D. Thomas, A. Nothofer, P. Sewell, and C. Christopoulos, "Modeling electromagnetic emissions from printed circuit boards in closed environments using equivalent dipoles," IEEE Trans. Electromagn. Compat., vol. 52, no. 2, pp. 462–470, May 2010.
11. Y. Liu, B. Ravelo, and A. K. Jastrzebski, "Time-Domain Magnetic Dipole Model of PCB Near-Field Emission," IEEE Trans. Electromagn. Compat., vol. 58, no. 5, pp. 1561–1569, Oct. 2016.
12. J.A. Russer and P. Russer, "An efficient method for computer aided analysis of noisy electromagnetic fields," in 2011 IEEE/MTT-S Int. Microw. Symp. - IMS, Baltimore, MD, 5-10 Jun 2011, pp. 1–4.
13. ——, "Modeling of noisy EM field propagation using correlation information," IEEE Trans. Microwave Theory Techn., vol. 63, no. 1, pp. 76–89, Jan 2015.
14. P. Russer, Electromagnetics, Microwave Circuit and Antenna Design for Communications Engineering, 2nd ed. Boston: Artech House, 2006.
15. D. Thomas, C. Obiekezie, S. Greedy, A. Nothofer, and P. Sewell, "Characterization of noisy electromagnetic fields from circuits using the correlation of equivalent sources," in 2012 Int. Symp. Electromagn. Compat. (EMC EUROPE), Rome, Italy, 17-21 Sep 2012, pp. 1–5.
16. A. Baev, A. Gorbunova, M. Konovalyuk, J. A. Russer, and Y. Kuznetsov, "Planar stochastic sources localization algorithm in EMC problems," in 2013 Int. Conf. Electromagn. in Adv. Appl. (ICEAA), Torino, Italy, 9-13 Sep 2013, pp. 1–4.
17. A. Gorbunova, A. Baev, M. Konovalyuk, Y. Kuznetsov, and J. A. Russer, "Stochastic EMI sources localization algorithm based on time domain planar near-field scanning," in Int. Symposium on Electromagnetic Compatibility (EMC EUROPE). IEEE, 2013, pp. 972–976.
18. A. Baev, A. Gorbunova, M. Konovalyuk, Y. Kuznetsov, and J. A. Russer, "Stochastic EMI sources localization based on ultra-wide band near-field measurements," in European Microwave Conference (EuMC), Nuremberg, 6-10 Oct. 2013, pp. 1131–1134.
19. A. Gorbunova, A. Baev, M. Konovalyuk, and Y. Kuznetsov, "Parametric reconstruction of stochastic EMI sources based on two-point planar near-field scanning," in Int. Symp. on Electromagn. Compat. (EMC Europe), Sep 2014, pp. 102–107.
20. J.A. Russer, G. Gradoni, G. Tanner, S. C. Creagh, D. Thomas, C. Smartt, and P. Russer, "Evolution of transverse correlation in stochastic electromagnetic fields," in Microwave Symposium (IMS), 2015 IEEE MTT-S International, May 2015, pp. 1–3.
21. M. Haider, A. Baev, Y. Kuznetsov, and J. A. Russer, "Near-field to far- field propagation of correlation information for noisy electromagnetic fields," in Proc. 48th Europe Microw. Conf., Madrid, Spain, Sep. 23-28 2018.
22. G. Gradoni, J. Russer, M.H. Baharuddin, M. Haider, P. Russer, C. Smartt, S.C. Creagh, G. Tanner, and D.W.P. Thomas, "Stochastic electromagnetic field propagation – measurement and modelling," Philosophical Transactions of the Royal Society A, p. 376(2134), Oct. 2018.
23. J.W. Goodman, Statistical Optics, John Wiley & Sons, Sep. 2000.
24. J.A. Russer and M. Haider, "Time-domain modeling of noisy electro- magnetic field propagation," in 2018 IEEE/MTT-S Int. Microw. Symp. - IMS, Philadelphia, PA, Jun. 10-15 2018, pp. 1013–1016.
25. J.A. Russer, M. Haider, and P. Russer, "Time-domain modeling of noisy electromagnetic field propagation," IEEE Transactions on Microwave Theory and Techniques, vol. 66, no. 12, pp. 5415–5428, Dec 2018.
26. J.A. Russer, N. Uddin, A. S. Awny, A. Thiede, and P. Russer, "Near- field measurement of stochastic electromagnetic fields," Electromagnetic Compatibility Magazine, IEEE, vol. 4, no. 3, pp. 79–85, 2015.
27. J.A. Russer, P. Russer, M. Konovalyuk, A. Gorbunova, A. Baev, Y. Kuznetsov, "Near-Field Propagation of Cyclostationary Stochastic Electromagnetic Fields," in International Conference on Electromagnetics in Advanced Applications (ICEAA), 7-11 Sept., p. 1456-1459, 2015.
28. J. A. Russer, P. Russer, M. Konovalyuk, A. Gorbunova, A. Baev, and Y. Kuznetsov, "Analysis of cyclostationary stochastic electromagnetic fields," in Int. Conf. Electromagn. in Adv. Appl. (ICEAA), 2015. IEEE, Sep 7-11 2015, pp. 1452–1455.
29. T. Asenov, J. A. Russer, and P. Russer, "Efficient characterization of stochastic electromagnetic fields using eigenvalue decomposition and principal component analysis method," in XXXIst URSI General Assembly and Scientific Symposium, Beijing, China, August 17-23 2014, pp. 1-4.
30. M, Haider, J.A. Russer, "Principal component analysis for efficient characterization of stochastic electromagnetic fields," in International Journal of Numerical Modelling, vol. 31, no. 4, 2017, DOI: 10.1002/jnm.2246.
31. P. Russer, "EMC measurements in the time-domain," Proc. 30th URSI General Assembly 2011, Istanbul, Turkey, 13–20 Aug. 2011.
32. J.A. Russer and S. Braun, "A novel vector near-field scanning system for emission measurements in time-domain," in IEEE International Symposium on Electromagnetic Compatibility (EMC), Pittsburgh, August 5-10 2012, pp. 462–467.
33. J. Russer, A. Frech, S. Braun, and P. Russer, "Spatially resolved measurement of radiated electromagnetic interference for mapping of noise sources and ambient noise cancellation," in 2012 Int. Conf. Electromagn. in Adv. Appl. (ICEAA), Sep. 2012, pp. 547–550.
34. M.A. Azpúrua, M. Pous, S. Cakir, M. Cetinta, and F. Silva, "Improving time-domain EMI measurements through digital signal processing," IEEE Electromagnetic Compatibility Magazine, vol. 4, no. 2, pp. 82–91, 2015.
35. M.A. Azpúrua, M. Pous, and F. Silva, "A measurement system for radiated transient electromagnetic interference based on general purpose instruments," in 2015 IEEE International Symposium on Electromagnetic Compatibility (EMC), Aug. 2015, pp. 1189–1194.
36. J.A. Russer, Y. Kuznetsov, and P. Russer, "Discrete-time network and state equation methods applied to computational electromagnetics," Mikrotalasna Revija (Microwave Review), pp. 2–14, July 2010.
37. J.A. Russer, A. Cangellaris, and P. Russer, "Correlation transmission line matrix (CTLM) modeling of stochastic electromagnetic fields," in 2016 IEEE MTT-S Int. Microw. Symp. (IMS), San Francisco, CA, U.S.A., May 22-27, 2016, pp. 1–4.
38. Y. Kuznetsov, A. Baev, M. Konovalyuk, A. Gorbunova and J. A. Russer, "Autocorrelation Analysis and Near-Field Localization of the Radiating Sources With Cyclostationary Properties," in IEEE Transactions on Electromagnetic Compatibility, vol. 62, no. 5, pp 2186-2195, Oct. 2020, DOI: 10.1109/TEMC.2019.2946748.
39. Y. Kuznetsov, A. Baev, A. Gorbunova, M. Konovalyuk, D. Thomas, C. Smartt, M. H. Baharuddin, J. A. Russer, and P. Russer, "Localization of the equivalent sources on the PCB surface by using ultra-wideband time domain near-field measurements," in Proc. EMC Europe, Wroclaw, Poland, 5-9 Sep, p. 1-6, 2016.
40. Y. Kuznetsov, A. Baev, M. Konovalyuk, A. Gorbunova, J. A. Russer, and M. Haider, "Time-domain stochastic electromagnetic field propagator based on Jefimenko's equations," in URSI Baltic Symposium, Poznan, Poland, May 14-17, 2018, pp. 188–191.
41. Y. Kuznetsov, A. Baev, A. Gorbunova, M. Konovalyuk, J.A. Russer, M. Haider, P. Russer, "Far-field Cyclostationary Characterization of Emissions from DUT Based on the Jefimenko's Equations," in 2019 International Symposium on Electromagnetic Compatibility (EMC Europe 2019), Barcelona, Spain, Sept. 2-6, p. 586-591, 2019.
42. A. Baev, Y. Kuznetsov, A. Gorbunova, M. Konovalyuk, J.A. Russer, "Modeling of Near-Field to Far-Field Propagator Based on the Jefimenko's Equations," in 2019 International Conference on Electromagnetics in Advanced Applications (ICEAA), Granada, Spain, 9-13 Sept., pp. 315-319, 2019.
43. D.J. Griffiths and M. A. Heald, "Time-dependent generalizations of the Biot–Savart and Coulomb laws," American Journal of Physics, vol. 59, no. 2, pp. 111–117, Feb 1991.
44. O.D. Jefimenko, "Solutions of Maxwell's equations for electric and magnetic fields in arbitrary media," American Journal of Physics, vol. 60, no. 10, pp. 899–902, Oct 1992.
45. O. Jefimenko, Electricity and Magnetism. New York: Appleton- Century-Crofts, 1966.
46. D.J. Griffiths, Introduction to Electrodynamics. Prentice-Hall, 1999.
47. A. Tankielun, U. Keller, E. Sicard, P. Kralicek, and B. Vrignon, "Electromagnetic Near-Field scanning for microelectronic test chip investigation," IEEE EMC Society Newsletter (October 2006), 2006.
48. N. Uddin, M. Spang, and A. Thiede, "Integrated magnetic loop probe in GaAs technology for active near-field sensor," in Microwave Conference, 2008. EuMC 2008. 38th European, Oct. 2008, pp. 1070–1073.
49. N. Uddin and A. Thiede, "Switchable double-sensor integrated active probe for near-field scanner," in Microwave Integrated Circuits Conference (EuMIC), 2011 European, Oct. 2011, pp. 37–40.
50. A. Thiede, N. Uddin, and A. Awny, "Integrated active miniature sensors for

electro-magnetic near-field measurement," in 2012 Asia-Pacific Symposium on Electromagnetic Compatibility (APEMC), May 2012, pp. 197–200.
51. Y. Kuznetsov, A. Baev, M. Haider, J.A. Russer, P. Russer, "Time-domain characterization of probes for two-point measurements of stochastic EM fields," in 2017 International Conference on Electromagnetics in Advanced Applications (ICEAA), Verona, Italy, 11-15 Sept., p. 1521-1524, 2017.
52. C. Smartt, D. W. P. Thomas, H. Nasser, M. Baharuddin, G. Gradoni, S. C. Creagh, and G. Tanner, "Challenges of time domain measurement of field-field correlation for complex PCBs," in 2015 IEEE International Symposium on Electromagnetic Compatibility (EMC), Aug. 2015, pp. 953–958.
53. D. Thomas, C. Smartt, H. Nasser, M. Baharuddin, S. Greedy, G. Gradoni, S. Creagh, and G. Tanner, "Time domain measurement of near-field emissions from complex PCBs," in European Microwave Conference (EuMC), Oct 2016, pp. 707–710.
54. J.A. Russer, M. Haider, M. H. Baharuddin, C. Smartt, S. Wane, D. Bajon, A. Baev, Y. Kuznetsov, D. Thomas, P. Russer, "Near-Field Correlation Measurement and Evaluation of Stationary and Cyclostationary Stochastic Electromagnetic Fields," in 2016 46th European Microwave Conference (EuMC), London, UK, 3-7 October, p. 481-484, 2016.
55. A. Baev, Y. Kuznetsov, A. Gorbunova, M. Konovalyuk, J.A. Russer, "Measurement Procedure for Cyclostationary Characterization of PCB Radiated Emissions," in 2019 International Conference on Electromagnetics in Advanced Applications (ICEAA), Granada, Spain, 9-13 Sept., pp. 320-324, 2019.
56. Y. Kuznetsov, A. Baev, A. Gorbunova, M. Konovalyuk, J.A. Russer, M. Haider, P. Russer, "Cross-correlation analysis of the cyclostationary near-field unintentional radiations from the PCB," in 2017 International Symposium on Electromagnetic Compatibility – EMC EUROPE, Angers, France, 4-7 September 2017.
57. Y. Kuznetsov, A. Baev, A. Gorbunova, M. Konovalyuk, J.A. Russer, M. Haider, P. Russer, "Cyclostationary Characterization of the Interference Induced by Crosstalk Between Transmission Lines," in 2019 International Symposium on Electromagnetic Compatibility (EMC Europe 2019), Barcelona, Spain, 2-6 Sept., p. 574-579, 2019.
58. A. Napolitano, Generalizations of Cyclostationary Signal Processing: Spectral Analysis and Applications, 1st ed. Hoboken, NJ, USA: Wiley, 2012.
59. Y. Kuznetsov, A. Baev, M. Konovalyuk, A. Gorbunova, M. Haider, J.A. Russer, "Cyclostationary Source Separation Based on Electromagnetic Measurements in the Near-field of PCB," in 2019 Progress in Electromagnetics Research Symposium (PIERS Rome 2019), Rome, Italy, June 17-20, pp. 1-8, 2019.
60. Y. Kuznetsov, A. Baev, M. Haider, J.A. Russer, P. Russer, "Time-domain far-field measurements for cross-correlation analysis," in 2017 International Conference on Electromagnetics in Advanced Applications (ICEAA), Verona, Italy, 11-15 Sept., p. 1517-1520, 2017.
61. IEC61967-3, Integrated Circuits, measurement of electromagnetic emissions, 150 kHz to 1GHz, Part3: Measurement of radiated emissions- Surface scan method, IEC standard, 2005.
62. T. Li, V. Khilkevich and D. Pommerenke, "Phase-Resolved Near-Field Scan Over Random Fields," in IEEE Transactions on Electromagnetic Compatibility, vol. 58, no. 2, pp. 506-511, April 2016.
63. G. Gradoni et al., "Near-Field Scanning and Propagation of Correlated Low-Frequency Radiated Emissions," in IEEE Transactions on Electromagnetic Compatibility, vol. 60, no. 6, pp. 2045-2048, Dec. 2018.
64. Atlys Spartanr-6 FPGA Trainer Board (LIMITED TIME). URL: https://store.digilentinc.com/atlys-spartan-6-fpga-trainer-board-limited-time-see-nexys-video/
65. Agilent Technologies. Jitter Analysis: The Dual-Dirac Model, RJ/DJ, and Q-Scale. White Paper 5989-3206EN. Santa Rosa, CA: Agilent Technologies, June 2005.

VII. Biographies

Yury Kuznetsov *(M'05–SM'09) received the Dipl.-Ing. degree in electrical engineering the Ph.D. degree in microwave and radar engineering, and the Doctor of Science degree in microwave and radar engineering, from the Moscow Aviation Institute (National Research University), Moscow, Russia, in 1974, 1981, and 2005, respectively. In 1974, he joined the Department of Radio Electronic, Moscow Aviation Institute (National Research University), where he has been a Research Engineer, and then a Senior Researcher in phased antenna arrays design, control systems development, and digital signal processing, until 1983. Since 1983, he has been an Assistant, and since 1985, he has been an Active Head of the Department of Theoretical Radio Engineering, Moscow Aviation Institute (National Research University) where he was an Assistant Professor from 1987 to 2001. In 2001, he was elected as a Professor and a Head of the Department of Theoretical Radio Engineering, Moscow Aviation Institute (National Research University). In 2007, he received the academic title Professor of the Theoretical Radio Engineering Department. He has authored or coauthored more than 180 scientific papers in refereed journals and conference proceedings and two books. Prof. Kuznetsov is a member of technical paper committees of Baltic URSI Symposium 2018 and EuMCE 2019, Chair of Baltic URSI Symposium 2020, Reviewer of EuMW, EMC Europe Conference, and MDPI journals. He was a recipient of the Best Paper Award from the EMC Europe 2019 Symposium.*

Andrey Baev *(M'06–SM'19) received the Dipl.-Ing. degree in 1999, and Ph.D. degree in 2002 in electrical engineering, both from the Moscow Aviation Institute (National Research University). In 1994, he joined the Theoretical Radio Engineering Department of the Moscow Aviation Institute (National Research University), where he has been a Research Engineer, then a Senior Researcher on digital signal processing and higher order statistics. In 2003 he has been elected as a Docent of the Theoretical Radio Engineering Department. From 2006 he is a head of R&D department on the Theoretical Radio Engineering Department of the Moscow Aviation Institute (National Research University). From 2005 to 2006 Andrey Baev was a supervisor of scientific work on electromagnetic compatibility. This research was supported by grants of Education and Science Ministry of Russian Federation. Dr. Baev joined the European Microwave Association (EuMA) in 2003 and the IEEE in 2006. He has authored or co-authored more than 150 scientific papers in refereed journals and conference proceedings and one book.*

Maxim Konovalyuk *received the Dipl.-Ing. degree in 2008, and Ph.D. degree in 2011 in electrical engineering, both from the Moscow Aviation Institute (National Research University). In 2012, he joined the Theoretical Radio Engineering Department of the Moscow Aviation Institute (National Research University) as an Assistant. Since 2014, he is a Docent of the Theoretical Radio Engineering Department. His current research interests include optimum signal processing, system identification, electromagnetic compatibility, and electromagnetic interference. He has authored or co-authored more than 60 scientific papers in refereed journals and conference proceedings.*

Anastasia Gorbunova *received the Dipl.-Ing. degree in 2011, and Ph.D. degree in 2014 in electrical engineering, both from the Moscow Aviation Institute (National Research University). In 2014, she joined the Theoretical Radio Engineering Department of the Moscow Aviation Institute (National Research University) as*

an Assistant. Since 2016, she is a Docent of the Theoretical Radio Engineering Department. Her research interests include system identification, digital signal processing, optimum signal processing, and electromagnetic compatibility. She has authored or co-authored more than 50 scientific papers in refereed journals and conference proceedings.

***Johannes A. Russer** (M'09) received the M.S.E.E. degree in electrical engineering and information technology from the Karlsruhe Institute of Technology, Karlsruhe, Germany, in 2003, the Ph.D.E.E. degree from the University of Illinois at Urbana–Champaign, Champaign, IL, USA, in 2010, and the Dr.-Ing. habil. Degree from the Technical University of Munich (TUM), Munich, Germany, in 2017. In 2004, he joined the University of Illinois at Urbana–Champaign as a Research Assistant. From 2007 to 2010, he was an Intern with Qualcomm Inc. In 2010, he joined the Institute of Nanoelectronics, TUM, as a Post-Doctoral Research Fellow, where he is involved in multiphysics modeling in nanoelectronics, quantum circuit theory, wireless power transfer, and in the area of stochastic electromagnetic fields. In 2017, he became associate professor (Privatdozent). He has authored or co-authored more than 200 scientific papers in refereed journals and conference proceedings. Johannes A. Russer is a member of VDE, IEEE, and the Eta Kappa Nu Honor Society. He is a recipient of the Best Student Paper Award at the IEEE International Microwave Symposium in 2008 and of the Best Paper Award from the ITG in 2015.*

***Peter Russer** (LF'13) received the Dipl.-Ing. (M.S.E.E.) degree in 1967 and the Dr. techn. (Ph.D.E.E.) degrees in 1967 and 1971, respectively, both from the Vienna University of Technology, Austria. In 1971, he joined the Research Institute of AEG-Telefunken in Ulm, Germany, where he worked on electronics and lightwave technology. From 1981 to 2008, Peter Russer has been Full Professor at the Technische Universität München (TUM), Germany. From October 1992 to March 1995 he also has been Director of the Ferdinand-Braun-Institut für Höchstfrequenztechnik, Berlin. After his retirement in 2008 he was appointed as Emeritus of Excellence at the TUM and since 2010 he is with the Institute of Nanoelectronics of the TUM. Peter Russer has published five books and more than 950 scientific papers in refereed journals and conference proceedings. In 1979, Peter Russer received the best paper award from the NTG (German Society for Information Technology). In 1994, he was elected Fellow of the IEEE. In 2006, Peter Russer was elected member of acatech, the German Academy of Science and Engineering. In 2006, he received the Distinguished Educator Award of the IEEE MTT Society and in 2009 the Distinguished Service Award from the European Microwave Association (EuMA). In 2007, Peter Russer received an honorary Doctor degree from the Moscow University of Aerospace Technologies (MAI). In 2010, Peter Russer has been awarded the Golden Ring of Distinction of the VDE - the German Association for Electrical, Electronic and Information Technologies.* **EMC**

What Exemplar LINK Means for You

Christian Thornton, Associate Editor,

iNARTE Business Manager

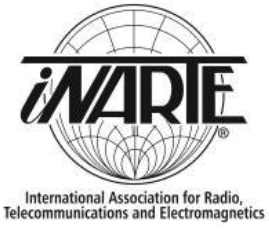

Last time I wrote to introduce Exemplar LINK, the new career pathways tool developed by iNARTE's parent company, Exemplar Global. Exemplar LINK is an innovative way for you to find and connect with colleagues, demonstrate your competence with digital badging and professional profiling, build your knowledge base through self-paced micro-training courses, and much more. Please click here to watch our short video explaining more about the Exemplar LINK concept.

For those of you working in EMC/EMI, ESD, product safety, or other related disciplines that make up the iNARTE community, Exemplar LINK will have a particular resonance. Engineers and technicians sometimes struggle to build community with colleagues who well understand the issues particular to this field. Perhaps you need feedback on a testing setup or questionable series of results. Maybe you want to find new training opportunities or explore different career pathways. Or it could be that you simply want to share your knowledge and demonstrate your competence to the industry at large. For these reasons, and many more, we have developed Exemplar LINK.

Too often in this highly technical profession we forget that our work is essentially human in nature—that means that although we must get the science right first and foremost, we also need to communicate our information for the good of our organizations, share our knowledge with others, and continually learn and grow individually and as a part of the broader community. It's not too grandiose to say that Exemplar LINK has been designed with these "soft skills" firmly in mind.

Exemplar LINK will replace the current iNARTE customer portal. Over the coming weeks you will hear more from us about Exemplar LINK and what this means for you and your certifications. The way you will access your new and improved customer portal, Exemplar LINK, will not change. Your details will be updated when first logging in when functionality for iNARTE customers is live in December.

Most of the content on Exemplar LINK is available for free or at very low cost. I encourage you to take a look, create your custom profile, and begin exploring all the many ways that this new tool can serve you in your career. We are always interested to hear your feedback as well, so please write us at admin@inarte.org to let us know what you think of Exemplar LINK or any of the other ways that we can serve you better! **EMC**